Repeated MRI scans of the human brain: diurnal oscillations in healthy adults and bipolar disorder patients

Matthew Carlucci[1,6], Tristram Lett[2], Sofia Chavez[3,4], Alexandra Malinowski[1], Nancy J. Lobaugh[3,5], Art Petronis[1,4,6,*]

[1]The Krembil Family Epigenetics Laboratory, The Campbell Family Mental Health Research Institute, Centre for Addiction and Mental Health, Toronto, Ontario, Canada, M5T 1R8

[2]Center for Population Neuroscience and Precision Medicine (PONS), Clinic for Psychiatry and Psychotherapy, Charité Universitätsmedizin Berlin, Berlin, Germany, 10117

[3]Brain Health Imaging Centre, Centre for Addiction and Mental Health, Toronto, Ontario, Canada

[4]Department of Psychiatry, Temerty Faculty of Medicine, University of Toronto, Toronto, Ontario, Canada

[5]Department of Medicine, Division of Neurology, Temerty Faculty of Medicine, University of Toronto, Toronto, Ontario, Canada

[6]Institute of Biotechnology, Life Sciences Center, Vilnius University, Vilnius, Lithuania, LT-10257

[*]corresponding author

Abstract

Regulation of biological processes according to a 24-hr rhythm is essential for the normal functioning of an organism. Temporal variation in brain MRI data has often been attributed to circadian or diurnal oscillations; however, it is not clear if such oscillations exist. We provide the first evidence that diurnal oscillations indeed govern multiple MRI metrics. We recorded cerebral blood flow, diffusion-tensor metrics, T1 relaxation, and cortical structural features every three hours over a 24-hr period in each of 16 male controls and eight male bipolar disorder patients. Diurnal oscillations were detected in numerous MRI metrics at the whole-brain level, and regionally. Rhythmicity parameters in the bipolar disorder patients were similar to the controls for most metrics, except for a larger phase variation in cerebral blood flow. The ubiquitous nature of diurnal oscillations has broad implications for neuroimaging studies and furthers our understanding of the dynamic nature of the human brain.

Key words: cosinor, MRI, circadian, diurnal, brain disease, bipolar disorder, cerebral blood flow, cortical thickness, cortical surface area, cortical volume, T1 relaxation, diffusion tensor imaging, fractional anisotropy, mean diffusivity.

Introduction

Cell-autonomous circadian oscillators and environmental cues such as light, sleep-wake, and feeding, interact across various animal tissues to produce diurnal rhythmicity[1]. Circadian and diurnal oscillations are an integral part of most biological processes including gene expression, metabolism, hormonal regulation, immune response, sleep, cognition and behavior[2,3]. Molecular oscillatory patterns are particularly complex in the brain, where different regions exhibit substantial variation in amplitudes and phases of oscillating RNA transcripts[4,5], metabolites[6], and proteins[7]. Yet, it is not clear if and how these periodic molecular effects translate into the larger-

scale structural and functional features in the living human brain, which can be measured by magnetic resonance imaging (MRI).

In PubMed, we identified over 500 articles matching search parameters: "diurnal OR circadian AND MRI AND brain". In many of these publications, scanning the same participants twice a day detected morning-evening differences in metabolism/cerebral blood flow[8,9] brain/parenchymal volume[10,11], diffusion metrics[12–15] and parameters derived from functional MRI[16,17]. These differences were not attributable to known MRI confounders such as technical differences in scanner type, image acquisition protocols, and data processing pipelines, nor to subject-related factors[10,11]. Therefore, it has often been assumed that these time-of-day effects reflect circadian or diurnal rhythmicity, but, in fact, their presence and parameters remain poorly understood. Thus far, the most direct experimental evidence for circadian oscillations in human MRI data comes from a functional MRI study that acquired several scans throughout the morning and night to test for changes in the brain's response to an attention task in conjunction with sleep deprivation[18]. To the best of our knowledge, no MRI studies to date have performed structural or quantitative imaging using an optimal design (sampling at evenly spaced intervals around the clock) to estimate 24-hr oscillations in the human brain.

The primary aim of the present investigation was to determine if 24-hr oscillations were present in an array of MRI metrics representing structural brain features and cerebral blood flow. Separation of endogenous (circadian) effects from those induced by environmental changes during day and night is not a trivial task, therefore we aimed to characterize diurnal rather than circadian rhythmicity.

Our secondary aim was to investigate if and how the oscillatory parameters differed in individuals affected by a brain disease. We recently suggested that disease may alter synchronous epigenomic circadian/diurnal oscillations[19,20], and this principle of desynchronosis is applicable to any other biological oscillator. Therefore, we additionally aimed to test the desynchronosis hypothesis in brain MRI metrics of patients affected with bipolar disorder (BPD), a common psychiatric disorder with numerous changes in circadian regulation[21].

In this study (Figure 1), we assessed 24 male participants (25-50yrs of age, 16 controls and eight BPD patients) each scanned every three hours over a 24-hr period, with the first scan beginning between 8:00 and 9:30. We derived nine MRI metrics from both standard and specialized MRI protocols (Methods) including arterial spin labeling, diffusion-tensor imaging, T1-weighted imaging, and T1 relaxometry. Each 30-min MRI session produced metrics of: cortical thickness (CT), cortical grey matter volume (GMV), cortical surface area (SA), white matter fractional anisotropy (WM-FA), mean diffusivity of white and grey matter (WM-MD, GM-MD), grey matter cerebral blood flow (CBF), and white and grey matter quantitative longitudinal relaxation time (WM-qT1, GM-qT1).

Cosinor regression sinusoidal curve fits[22] (Methods) were applied to the brain-derived metrics, at the whole brain and regional level, to detect diurnal oscillations and estimate their parameters. We examined the MRI metric variation explained by the group-level oscillations and identified instances where oscillations were not synchronous across subjects. The analyses were extended to compare the BPD group with the controls.

Results

Participants

Twenty-four participants completed the study (Supplementary Fig. 1). Our inclusion criteria included both sexes; however, all participants were males. Six females expressed initial interest, and three were eligible, but due to scheduling challenges and the onset of the COVID-19

lockdown of the research facility, none participated. Six of the eight BPD patients recruited were being treated with a mood stabilizer (lithium, carbamazepine, lamotrigine, or valproic acid) at the time of scanning. One patient was medication-free, but had a history of treatment with valproic acid, and one patient's medication information was not disclosed. All patients were in remission at the time of recruitment and during their scanning session. Their euthymic states were confirmed using the Young Mania Rating Scale (YMRS)[23] approximately 30 days prior to enrolment (mean[SD]=30[16] days, range=11-58 days). Apart from one Asian in the control group, the ethnic background of all participants was Caucasian. To ensure a streamlined experience for the patients, the first four scanning sessions were controls only, the next four sessions included patients (Methods). Controls and BPD patients were similar in terms of most characteristics, including their Pittsburgh Sleep Quality Index[24] (PSQI) and sleep schedules in the week prior to scanning (Table 1).

Technical variation

CBF or diffusion scans were repeated back-to-back three times at each of the nine time points in two control subjects per measure. Temporal variation across the 24-hr period was consistently significantly larger than within time point technical (scan-to-scan) variation for the relevant whole-brain metrics (CBF, GM-MD, WM-MD, and WM-FA; one-way ANOVA range $F_{8,18}[p]=5.8[9.4\times10^{-4}]$ to $22[7.8\times10^{-8}]$; Supplementary Table 1).

Diurnal oscillations in the whole brain averages of control subjects

Whole-brain diurnal oscillations were tested with a two-stage cosinor model[22] (Methods) with a 24-hr period (Figure 1a). Briefly, a subject-level cosinor regression model (referred to as S-cosinor going forward) was fit to each control subject's data to obtain subject-specific parameter estimates for: the midline estimating statistic of rhythm (MESOR), the oscillation amplitude, and the time of its peak (acrophase). These individual fits are shown in Figure 2a. Then, an average group-level cosinor model (referred to as G-cosinor going forward) was obtained by averaging S-cosinor parameters[22] (Methods). The corresponding G-cosinor zero-amplitude F-test revealed that four of the nine imaging-derived MRI metrics exhibited significant group-level 24-hr oscillations (Supplementary Table 2). In order of acrophase time these were: WM-MD ($F_{2,14}$=10.5, p=0.0017, acrophase=13hrs), GM-MD ($F_{2,14}$=9.5, p=0.0025, acrophase=16hrs), WM-FA ($F_{2,14}$=8.8, p=0.0034, acrophase=18hrs), and CBF ($F_{2,14}$=6.8, p=0.0088, acrophase=21hrs). Individual acrophases and corresponding significant group-level acrophases with their 95% confidence intervals (CIs) are shown in Figure 2b, and a summary of diurnal oscillation amplitudes and other related statistics for each significant MRI metric are presented in Table 2.

The proportion of variance explained (R^2) by these diurnal oscillations was assessed under two contexts. First, we proceeded without adjusting for inter-individual variation in subjects' MESORs to obtain an unnormalized R^2 (R^2_{UN}). Here, we utilized the G-cosinor MESOR, amplitude, and acrophase to model the data. The CBF G-cosinor model explained the most total variance (R^2_{UN}=0.020), followed by WM-MD (R^2_{UN}=0.0098), GM-MD (R^2_{UN}=0.0055), and WM-FA (R^2_{UN}=0.0034) (Figure 2c). Second, the proportion of variance explained by diurnal oscillations was assessed after controlling for inter-individual variation by demeaning the data within each subject. This effectively set the MESOR to zero, and we utilized only the amplitude and acrophase estimates of the G-cosinor model. The proportion of remaining variance in the demeaned data (demeaned R^2; R^2_{DM}) explained by diurnal oscillations increased by about an order of magnitude compared to R^2_{UN}, with the largest in GM-MD (R^2_{DM}=0.20), followed by WM-MD (R^2_{DM}=0.19), CBF (R^2_{DM}=0.15), and WM-FA (R^2_{DM}=0.084) (Figure 2d).

No significant group-level diurnal oscillations were found for CT, GMV, SA, GM- and WM-qT1, which suggested that these metrics were static, or oscillations were too small to be detected with the current sample size (this is further explored in the BPD section). Alternatively, within-subject diurnal oscillations may have been real, but out of phase across individuals, i.e., asynchronous oscillations. In this case, aggregation of widely dispersed individual acrophases would have led to a G-cosinor amplitude too low to produce significant group-level oscillations (Figure 1b, II). To test this alternative possibility, we utilized the S-cosinor p-values and Fisher's meta-analytic method[25] to estimate the accrued evidence for subject-level diurnal oscillations (Methods). This acrophase-agnostic test was significant for both GM-qT1 ($p=0.0042$) and WM-qT1 ($p=0.042$), but not for CT, GMV, and SA (Supplementary Table 2).

To provide context to the observed oscillations in the brain with non-brain metrics known to oscillate diurnally, we also measured subjects' body weights prior to each scan session. Weight exhibited strong evidence for 24-hr oscillations with its acrophase around midnight (G-cosinor $F_{2,14}=32$, $p=5.7\text{x}10^{-6}$, acrophase=24hrs, $R^2_{UN}=0.00041$, $R^2_{DM}=0.38$, Figure 2e-h, Table 2), which was very similar to previously published results[26]. Body weight co-varies with total body water[26], and direct experimental manipulation of water intake results in changes to brain volumes[27,28] and quantitative MRI metrics (SC, 2017, https://cds.ismrm.org/protected/17MProceedings/PDFfiles/1001.html). Based on such findings, body weight has been used as a proxy for hydration status[14]. In our study, including subject weight as a covariate did not eliminate oscillatory effects; all four MRI metrics remained significant (all G-cosinor $p<0.05$; Supplementary Table 3).

Diurnal oscillations in brain regions of control subjects

We partitioned the brain into predefined regions of interest (ROIs) to test whether diurnal oscillation characterization remained feasible at the regional-level. Briefly, CBF, GM-MD, GM-qT1, SA, CT, and GMV values were obtained from 358 cortical grey matter ROIs using the Human Connectome Project Multi-Modal Parcellation cortical atlas[29] (version 1.0), an additional 14 subcortical ROIs from the Freesurfer automatic segmentation atlas[30] were obtained for CBF, GM-MD, and GM-qT1; WM-MD, WM-FA, and WM-qT1 values were obtained from 46 skeletonized white matter ROIs using the Johns Hopkins University diffusion-based white-matter atlas[31] (Methods).

We found significant evidence of regional diurnal oscillations using identical methods to whole-brain analysis, for each ROI. S-cosinor regression was first applied for every subject, MRI metric, and ROI, independently (Figure 3a; Supplementary Fig. 2). Resulting group-level oscillations were nominally significant (G-cosinor $p<0.05$) in 5.9% to 85.8% of ROIs across seven of the nine MRI metrics (Supplementary Table 4). After false-discovery rate (FDR) adjustment, we obtained significant ($q<0.05$) regional diurnal oscillations for CBF, GM-MD, and WM-MD (289, 53, and 3 ROIs, respectively; Figure 3b-c). The acrophases of these ROIs ranged from 18-23hrs in CBF, 14-20hrs in GM-MD, and 8-18hrs in WM-MD. These regional acrophases were generally within the 95% confidence interval (CI) of their respective whole-brain acrophases; maximal ROI differences from the whole-brain acrophases were 3hr for CBF (whole-brain CI spans 3hrs), 4hr for GM-MD (CI spans 4hrs), and a 5hr difference originating from two of the three oscillating WM-MD ROIs (CI spans 4hrs) (Figure 3c; Table 2). R^2_{UN} effect sizes were distributed around their observed whole brain R^2_{UN} values, with ROIs reaching $R^2_{UN}=0.047$, 0.030, and 0.028 for CBF, GM-MD, and WM-MD, respectively. After within-subject demeaning, ROI R^2_{DM} were lower than their observed whole brain R^2_{DM} on average, yet maximum R^2_{DM} were near whole brain observations at $R^2_{DM}=0.21$, 0.21, and 0.13 for CBF, GM-MD and WM-MD,

respectively (Table 2). These regional diurnal oscillation statistics are shown in Supplementary Fig. 3.

The remaining metrics did not exhibit group-level oscillations at the regional level. We observed that the regional acrophases for GM-qT1 (Figure 3a) and WM-qT1 (Supplementary Fig. 2) were clustered within each subject, but these clusters were dissimilar across subjects. This suggested that individual diurnal oscillations were present regionally, but group-level regional oscillations were undetectable due to the highly variable acrophases across subjects. The follow-up acrophase-agnostic test detected 40.6% and 8.7% of ROIs with nominally significant evidence for subject-level diurnal fits in GM-qT1 and WM-qT1, respectively, with 4 ROIs surviving FDR adjustment ($q<0.05$) in GM-qT1 (Supplementary Table 4).

Diurnal oscillations in bipolar disorder

After establishing diurnal oscillations in controls, we turned our attention to the group of eight patients diagnosed with BPD. We first established that neither their diurnal actigraphy or body weight oscillatory parameters differed from the controls (Table 1; Supplementary Fig. 4). Next, we interrogated the BPD MRI data for evidence of oscillations (Figure 4a), assessed how similar the detected oscillations were compared to the controls, and then combined the two datasets to increase the sample size for further oscillation detection (Figure 4a-c). Finally, we followed up on evidence for desynchronosis in CBF and its related implications to disease studies (Figure 4d-e).

At the whole-brain level, the BPD group exhibited significant 24-hr rhythmicity for GM-MD and WM-FA (G-cosinor $F_{2,6}=6.9$, $p=0.027$, and $F_{2,6}=21.3$, $p=0.0019$, respectively; Figure 4a). Acrophase times for the two metrics in BPD (15hrs and 17hrs, respectively) did not differ from the control group (16hrs and 18hrs, respectively; permutation $p=0.77$, and $p=0.68$, respectively; Methods). Taken together, these findings argue that oscillations were not altered in BPD for GM-MD and WM-FA.

Several MRI metrics did not show evidence for group-level whole-brain oscillations (BPD: CBF, WM-MD; controls: SA; both: GMV, CT, WM- and GM-qT1). We assumed that there may have been inadequate power to detect oscillations. If subthreshold oscillatory signals had similar acrophases, they could become significant when assessed in a combined cohort of all 24 subjects. Combining the groups indeed strengthened the evidence for oscillations in WM-MD (G-cosinor; $F_{2,22}=13.9$, $p=0.00012$ compared to $F_{2,14}=10.5$, $p=0.0017$ in controls only) without changes in the acrophase (13hrs)(Figure 4a). New evidence for oscillations, unseen in the controls alone, was detected for SA ($F_{2,22}=6.7$, $p=0.0053$, acrophase=4hrs). GMV, initially considered to be arhythmic in both groups, now revealed evidence for oscillations in the combined sample ($F_{2,22}=3.8$, $p=0.038$; acrophase=6hrs). Similar to the control-only analysis, the group-level test in the combined sample was non-significant for both qT1 metrics, yet the acrophase-agnostic test further supported the presence of asynchronous diurnal oscillations in GM- and WM-qT1 ($\chi^2=72$ and $\chi^2=62$; $p=0.0013$ and $p=0.015$, respectively). The single remaining arhythmic measurement was CT, which did not show evidence of synchronous or asynchronous oscillations (Figure 4a; Supplementary Table 2).

At the brain regional level, the BPD cohort alone produced only five significantly oscillating ROIs (G-cosinor FDR $q<0.05$; all in WM-FA), likely due to the cohort's small sample size. Adding this cohort to the controls, however, dramatically increased the number of significant ROIs in many metrics compared to the controls only (Supplementary Table 4). G-cosinor detected an additional 117 and 8 ROIs for GM-MD and WM-FA (Figure 4b), plus 17 new ROIs for CBF (despite 24 fewer ROIs overall; Supplementary Table 4) in the combined sample. The acrophase-agnostic test revealed 93 new ROIs (FDR $q<0.05$) for GM-qT1 (Figure 4c), plus 119, 101, and 2 additional ROIs for CBF, GM-MD, and WM-MD, respectively (Supplementary Table 4).

Some key whole-brain CBF observations suggested the presence of group-wise differences and prompted a follow-up analysis. Unlike the controls, CBF in the BPD patients did not show group-level oscillations (G-cosinor p=0.74), and adding their data to the control data did not appreciatively change the statistical evidence for oscillations (combined p=0.0090 *vs.* controls-only p=0.0088). Two explanations for the lack of significance of a CBF group-level oscillation in the BPD-only analysis were considered: 1) a loss of individual oscillations in the BPD patients (Figure 1b, III), or 2) a loss of acrophase consistency relative to controls, i.e., desynchronosis (Figure 1b, II). Our analyses did not detect evidence for the first possibility; individual CBF oscillation strengths in the BPD patients did not differ from those in the controls (differential R^2 of the within-subject S-cosinor fits; two-sided Welch's t-test, t(15)=0.39, p=0.70), indicating no loss of individual oscillations in BPD. In support of the second possibility, the acrophases of the BPD patients were widely distributed around the clock (Figure 4a). The BPD acrophase variance was significantly larger than the controls (acrophase variance=0.77 and 0.32 in patients and controls, respectively; permutation p=0.017; Methods). Therefore, we concluded that desynchronosis contributed to the lack of a BPD group-level oscillation. Interestingly, the magnitude of each BPD patient's acrophase deviation from the combined cohort strongly correlated with their subjective sleep quality score (PSQI, Pearson's r=0.91; two-sided p=0.0015; Supplementary Fig. 5).

The absence of CBF group-level oscillations in BPD patients, but presence of such in the controls, translated into a novel disease-related time-of-day effect. To put this finding in the context of cross-sectional studies, we compared the means of the patients and controls at each time point and showed that the magnitude of CBF differences exhibited a significant oscillation (cosinor F-test p=0.0025; Figure 4d-e). The differences in whole-brain blood flow in the BPD group changed two-fold from 9 ml g^{-1} min^{-1} below controls at 8hrs to 18 ml g^{-1} min^{-1} below controls at 21hrs. In contrast, for metrics where oscillations did not differ between the two groups, group-wise differences were stable across the 24-hr period (e.g. GM-MD, cosinor F-test p=0.92; Figure 4d-e).

Discussion

In this study, we have shown 24-hr oscillations in eight of nine human brain measurements. Many of these phenomena have been discussed frequently in the literature, but were not formally identified prior to this study. Two statistical approaches, G-cosinor modeling and the acrophase-agnostic test, identified two facets of oscillation: one where the oscillations were synchronous across subjects at the group level (G-cosinor), and one where oscillations were strong at the individual level (S-cosinor), but asynchronous across subjects. The two effects are not mutually exclusive, and most G-cosinor significant metrics were also significant in the acrophase-agnostic test. On the other hand, WM- and GM-qT1 exhibited strong subject-level diurnal effects detected only by the acrophase-agnostic test.

Diurnal oscillations in the brain exhibited several interesting features across the MRI metrics, individuals, and brain regions. In the whole brain, a non-negligible proportion of the total variance was explained by diurnal oscillations across MRI metrics (R^2_{UN}=0.34%-2.0%). On the other hand, when inter-subject variability in steady-state values was removed, the model explanatory power improved, and diurnal oscillations were shown to be a substantial source of within-subject variation (R^2_{DM}=8.4%-20%). All other factors being equivalent, data acquired in a typical cross-sectional neuroimaging study will reflect the combination of differences in the MESOR and the presence of oscillations. These effects may vary spatially (Supplementary Fig. 3), and certain brain regions may show stronger oscillations than others. Considering oscillations such as these, and their regional variation, can reduce variability and biases in populational MRI studies.

Evidence for 24-hr oscillations provides new insights into the common, but previously experimentally unproven, interpretation that time-of-day effects are fragments of circadian/diurnal variation e.g., diffusion metrics in WM[13]. Technical and methodological disparities prohibited direct comparisons of our findings with the existing time-of-day literature, yet our oscillatory models may help explain the origins and variability of morning-evening differences. Demonstrably, if an acrophase (or nadir) occurs around noon (e.g. WM-MD; acrophase=13hrs) morning-evening differences may be sensitive to scanning time (Figure 5, red arrows). Here, even small changes in the timing of morning and evening scans can lead to inconsistent results. Time-of-day effects in other MRI metrics may be less sensitive to scan times, e.g., in WM-FA (acrophase=18hrs), where evening scans would consistently produce a stronger signal compared to morning scans (Figure 5, black arrows).

Our findings provide a foundation to guide designs (e.g., scan timing and sample sizes) for future studies of oscillations in the brain. We demonstrated that, after adding the BPD group to the controls, new oscillating ROIs were identified at the group-level (GM-MD and WM-FA; Figure 4b), and subject-level (CBF, GM-qT1, and GM-MD; Figure 4c). ROI oscillation maps for most brain metrics, however, remained sparse, indicating that larger studies are necessary for identification of new diurnal effects at regional and/or voxel-based resolution.

Subject- or population-specific diurnal oscillations of MRI-based brain features may help to uncover etiopathogenic mechanisms of neuropsychiatric disease. As exemplified by CBF, oscillation characteristics can differ significantly in BPD patients compared to controls. CBF desynchronosis points to diurnal shifts in metabolic demand and adds to the numerous molecular[21] and behavioral[32] facets of circadian/diurnal dysregulation in BPD. A subset of BPD patients, however, exhibited CBF acrophases within the acrophase range of control subjects, which may indicate a stable remission. Alternatively, a large acrophase deviation from the norm may indicate poorly controlled remission or perhaps even a looming relapse of disease. The preliminary link between objective acrophase measures and the patient-reported sleep quality (Supplementary Fig. 5) may help uncover the mechanisms of disturbed sleep and hallmark BPD relapse[33].

There are some limitations of our study, some of which can be addressed in the future. First, due to restrictions during the COVID-19 lockdown era, we were not able to scan female subjects and the sample size of BPD patients was limited to eight. Second, we did not control for the impact of nutrition, exposure to light, seasonal variation, and other Zeitgebers, which could have differentially impacted the BPD and control cohorts. However, the observed similarities in diurnal MRI metrics between groups and across subjects argues against substantial externally induced biases. Third, the array of medications taken by the BPD patients may have affected their diurnal oscillations. Fourth, our study was not sufficiently powered to perform some comparisons, such as ROI oscillations, either across regions or across the two groups, both of which are of critical importance for uncovering the brain disease topography. Finally, waking up multiple times during the night for scanning disrupted sleep patterns and may have confounded MRI measurements. This limitation, however, is hard to address when studying the living human brain.

Mapping individual-specific rhythms may help address a major drawback of traditional cross-sectional studies, especially in clinical populations: there is abundant evidence that group-averaged measurements poorly represent individual disease[34]. MRI desynchronization parameters may provide the basis from which to establish novel biomarkers, subsequently enabling the stratification of disease subtypes and explaining the contradicting results of chronotherapeutics[35]. Patient-specific brain-regional and/or temporal features of disease may become of particular importance in the personalization of targeted therapeutic approaches such as deep brain stimulation.

Methods

Data Collection

Participants

Participants were considered for inclusion if they were between 18-50yrs of age and met the inclusion criteria for their group. Exclusion criteria that applied to all participants were: pregnancy, blindness, metabolic disease (e.g., diabetes), dieting, and contraindications to MRI. All assessments were performed at the Centre for Addiction and Mental Health (CAMH) in Toronto, ON, Canada.

Controls. Individuals were recruited via word-of-mouth referrals, existing study registries and advertisements. Inclusion criteria were: no history of alcohol or substance use disorders, psychiatric disorders, neurological disorders or sleep disorders. Smoking was not an exclusion criterion due to the frequent consumption of nicotine products in the BPD patients.

Patients. Patients were recruited from existing patient registries and databases at CAMH. The same inclusion/exclusion criteria used for controls applied to the BPD group, with the exception of a history of psychiatric disorder. To be included, a diagnosis of BPD-I or BPD-II was required, which was confirmed using the Mini-International Neuropsychiatric Interview[36] (MINI). The Young Mania Rating Scale (YMRS) was administered to confirm the patients were euthymic.

The CAMH Research Ethics Board approved the study, all participants provided written informed consent prior to commencement of the study, and in accordance with the Declaration of Helsinki.

General Procedures

During the week prior to the scanning sessions, participants wore a FitBit Flex™ for a minimum of 3 days to achieve 3 full days of recordings (see "Actigraphy"). All participants completed the PSQI at the time consent was obtained. On the day of scanning, participants arrived at the CAMH imaging facility between 7:00 and 9:00, approximately one hour before their first scan. Participants changed into a surgical gown/pants and were provided private rooms, which included a desk and bed for the duration of the ~25-hr study. Each subject was scanned every three hours for a total of nine ~30-min MRI sessions; scheduled scan start time was assigned to the session. In between scanning sessions, participants had access to regular meals (9:30-10:30, 13:30-14:30, and 19:30-20:30), snacks, water and coffee (all of which were recorded), and were permitted to go about their regular activities while on site (including work, leisure, eating and sleeping).

During the preparation phase (September 2017-August 2018), we decided which MRI metrics should be interrogated, optimized the scan frequency, which initially was set to be every 6 hrs but after preliminary analysis, was changed to every 3 hrs, and resolved various logistical issues related to the ~25-hr experiment. All scan sessions were performed over 8 weekends, from Saturday morning to Sunday morning, spread over a 15-month period from November 2018 to February 2020. Control subjects were scanned from November 2018 to August 2019. Recruitment of BPD patients was launched in January 2019, after evidence of diurnal oscillations for several MRI metrics was detected in the controls. Without such evidence, collection of data from patients would have not been justified. Therefore, BPD patients were scanned from August 2019 to February 2020.

Actigraphy

The FitBit data were acquired primarily to confirm self-reported sleep durations and PSQI (reported in Table 1); we did not attempt to assign a "chronotype" to each person. Upon consent into the study, participants were provided with a Fitbit Flex 2 (firmware 24.24.30.2) and were requested to wear the device for 4-5 full days prior to the study date. Upon receipt of the device,

participants were guided to download the official Fitbit smartphone app from the corresponding (Android or iOS) app store, and were instructed to synchronize their device data every six hours with the corresponding account. A final synchronization was performed on the morning of the study at which time the devices were returned. Device data were extracted from the official Fitbit website using the "Request Data" export function (February 2020), and were obtained in JSON format. Sleep-wake cycles and by-minute step data were included in the raw exported data. Step data were extracted from the raw download step JSON files where 72 hours of contiguous data (3 days starting from midnight) were obtained for each subject. Data were imported as Greenwich Mean Time (GMT) and converted to their respective Toronto time. One participant's actigraphy data were collected for the five days following the study visit due to synchronization issues.

Image acquisition

MRI data were acquired using a 3.0-Tesla GE Discovery MR750 (General Electric Medical Systems, Milwaukee, WI, USA). Each MRI session included the following acquisitions: T1-weighted imaging (3D BRAVO, sagittal slices, 0.9 mm^3 voxels, echo time: 3.02ms, repetition time: 6.77ms, flip angle: 8°), 3D pseudo-continuous arterial spin labeling imaging (pCASL, 3.0mm^3 voxels, axial slices, echo time: 11.11ms, repetition time: 5050ms, flip angle: 111°, post-label delay: 2025ms), diffusion-weighted imaging (b-value=1000, 2mm^3 voxels, 32 diffusion directions; posterior to anterior encoding direction; four b-value=0, repetition time ~7142ms). An 8-volume non-diffusion weighted sequence was also acquired with the same parameters, but with the encoding direction anterior to posterior for B0-induced distortion correction. Four acquisitions were used to calculate calibrated quantitative T1 relaxation time maps with B1 correction[37] (sagittal slices, two high resolution (1mm^3) fast spoiled gradient echo (fSPGR) scans with whole-brain excitation, echo times: 4.4ms; repetition times 10.6ms; and flip angles of 3°(Flip3) and 14° (Flip14); two lower resolution (4mm^3) SPGR scans with repetition times 50-60ms, echo time 5ms, flip angles 130° and 150°).

Technical variation

To measure variance due to scanner performance (technical variation), DTI and ASL measurements were each repeated three times (15-18 minutes of acquisition time) at each of the nine time-points. On the same scanning day, DTI and ASL were repeated for two separate pairs of subjects (Diffusion: C027 and C029; CBF: C028 and C031). For those subjects, the quantitative T1-mapping protocol was dropped to accommodate the extra scans, and their second DTI or ASL scans were used for all other analyses.

Image Processing

T1-weighted. Following N4 bias correction[38], unbiased (equidistant from all sources) within-subject T1-weighted templates were created using all T1-weighted images for each subject (nine images per subject) to create 24 individualized templates with the Freesurfer (version 7.1.1) mri_robust_template script[39]. Each subject's T1-weighted image was linearly registered to their respective template image using Advanced Normalization Tools (ANTs) version 2.3.3 (http://stnava.github.io/ANTs)[40]. For each registered T1-weighted image, brain extraction was performed using the antsBrainExtraction.sh script and the OASIS-30 Atropos template[41]. Cortical reconstruction was performed on all T1-weighted images using the Freesurfer image analysis suite (http://surfer.nmr.mgh.harvard.edu). After Freesurfer's recon-all step1, the ANTs brain extracted mask was applied to Freesurfer's watershed brain mask to provide a tighter brain extraction for surface creation. Each brain extraction was manually checked, and the final steps of recon-all were performed.

Diffusion. Diffusion-weighted images (DWI) were processed using FSL 6.0.3. Eddy current correction and echo-planar B0-induced imaging distortion correction were performed using the phase-encode reversed non-DWIs (b=0) with 'topup' and 'eddy'[42]. FSL's 'dtifit' was used to calculate fractional anisotropy (FA) and mean diffusivity (MD). For registration purposes, unwarped average non-DWIs were calculated, and within-subject unbiased non-DWI templates were created using the mri_robust_template. Subject-specific tract-based spatial statistics (TBSS)[43] skeletons were created using a modified version of TBSS (https://github.com/trislett/ants_tbss) that implements ANTs linear and non-linear transformations for skeletonization instead of FSL's FLIRT and FNIRT. For the mean FA image, a FA cutoff of 0.2 was applied to create the mean FA skeleton. The unbiased, within-subject non-DWI template also underwent linear and non-linear transformations to the subjects' N4-corrected T1-weighted image to transform the MD images into native T1-weighted space. Technical issues were identified for C063, session 2, so all of their MRI metrics were reduced to 8 time points.

Cerebral blood flow. The default CBF maps calculated by the scanner software were used for analysis. The 'difference images' (untagged-tagged) generated by the scanner software first underwent linear and non-linear registration to the brain-extracted non-DWI (b=0) template for each subject. The CBF maps were then transformed to non-DWI template space, and the CBF maps were transformed to the unbiased T1-weighted volume using the same transformation used to move the subject's MD images to T1-weighted space.

Quantitative T1 mapping. All four SPGR images used to create the qT1 maps were first reoriented and transformed into the space defined as halfway between the Flip3 and Flip14 images using the "halfway_flirt" command from FSL's SIENA pipeline. The transformed Flip3 image was brain-extracted using FSL's 'bet' (Brain Extraction Tool) and the resulting mask was used to extract the brain of the reoriented Flip14 image. B1 maps were generated using the two high flip angle scans via the method of slopes[44], and qT1 maps were computed using the variable flip angle method with a B1 correction[44] and calibration procedure[37]. Linear and non-linear transformations of the qT1 maps to the unbiased T1-weighted subject images were performed and the qT1 maps were transformed to template space using the T1-weighted unbiased subject to MNI152 1mm space linear and non-linear transformations. qT1 data quality was deemed to be not usable due to participant motion for one subject (C056) on their ninth scan, so their qT1 data were reduced to 8 time points.

Regions of Interest

Grey matter ROIs. The Human Connectome Project Multi-Modal Parcellation atlas[29]; version 1, HCP_MMP1) was applied to the Freesurfer cortical tessellation to generate 358 cortical regions of interest (ROIs) to extract regional cortical thickness (CT), surface area (SA), and grey matter

volume (GMV). To generate mean regional CBF, GM-MD, and GM-qT1 values, ROIs from the HCP_MMP1 atlas were transferred into each subject's T1-weighted space using multiAltasTT (https://github.com/faskowit/multiAtlasTT) incorporating FreeSurfer gaussian classifier surface atlases[45]. For GMV, GM-MD, CBF, and GM-qT1, 14 additional subcortical regions were obtained using Freesurfer's automatic segmentation (aseg) of bilateral thalamus, caudate, putamen, amygdala, pallidum, and accumbens[30]. Bilateral hippocampus was included in both the HCP_MMP1 and the Freesurfer atlases; the Freesurfer parcellation was used. Mean CT, mean GMV, and total SA from the Freesurfer vertices were used to generate the measures for whole-brain analyses. A whole-brain cortical grey matter mask was derived from all HCP_MMP1 atlas regions and was used to calculate mean grey matter values for CBF, GM-MD, and GM-qT1. The whole-brain mean grey matter measures do not include the Freesurfer subcortical parcels.

White matter ROIs. The parcellations from the Johns Hopkins University DTI-based white-matter ICBM atlas[46]; JHU ICBM DTI-81; JHU_ICBM) were used to define 46 white matter ROIs on the TBSS skeleton and to extract regional and whole-skeleton mean white matter MD (WM-MD), FA (WM-FA), and WM-qT1 (Supplementary Fig. 6). Note that bilateral tapetum was not included due to missing data in some subjects. For all metrics, data were obtained from the TBSS skeleton and ROIs in native T1-weighted space. For consistency with the description of the grey matter whole-brain results, whole-skeleton measures are referred to as 'whole-brain' in the main text.

Units

Unless otherwise indicated, metrics are in units as follows: CBF, ml g^{-1} min^{-1}; GMV and subcortical volume, 10^3 mm^3; SA, 10^3 mm^2; CT, mm; FA, unitless [1]; MD, 0.1 mm^2s^{-1}; qT1, ms.

Data Analysis and Statistical Methods

Subject-level oscillations (S-cosinor)

For each subject, cosinor linear regression was fitted with a 24-hr period to detect diurnal oscillations[22]. The data were modeled by linear cosine and sine transformations of MRI acquisition time (t) to arrive at a model for MESOR, amplitude, and acrophase, starting with the following formula:

$$y = \beta_0 + \beta_1 \cos(\frac{2\pi t}{\tau}) + \beta_2 \sin(\frac{2\pi t}{\tau}) + error$$

where t is MRI acquisition time, τ is the period (24-hr). The intercept coefficient (β_0) is the MESOR. β_1 and β_2 are regression coefficients that were used to calculate the amplitude (A) and acrophase as:

$$A = \sqrt{\beta_1^2 + \beta_2^2} \qquad acrophase = \text{atan2}(\beta_1, \beta_2)\frac{\tau}{2\pi}$$

Such that $y = \beta_0 + A \cos((t - \text{acrophase})2\pi/\tau) + \text{error}$. Each subject's p-values for the significance of diurnal oscillations were determined by the F-test comparing the cosinor model to an intercept-only (null) model and were used for the acrophase-agnostic test (described below). R^2 of these within-subject models were obtained for each subject and used for the CBF differential oscillation strength test.

Group-level oscillations (G-cosinor)

The population-mean cosinor[22] approach was applied with the aim to make inferences regarding a populational average rhythm for each group, and is referred to as G-cosinor throughout the text. This is a two stage model where first stage estimates were obtained by fitting each subjects' data

to the S-cosinor model described above. Next, across subjects, the coefficients were averaged to obtain: β_0^* (MESOR), β_1^* and β_2^*, and the following group-level model:

$$\hat{y} = \beta_0^\star + A^\star cos(t - acrophase^\star)$$

Where "*" indicates a population mean estimate, and A^* and acrophase* were derived from β_1^* and β_2^*. In this procedure, S-cosinor $[\beta_1,\beta_2]$ values were considered jointly. A single hypothesis test was performed with the null that the true population mean values are zero (i.e., $[\beta_1^*,\beta_2^*] = [0, 0]$) or equivalently, that $A^*=0$. The p-value was obtained by the corresponding multivariate F-test[22] and is referred to as G-cosinor p-value throughout the text. In the regional analyses, for each metric, correction for multiple comparisons was performed using the Benjamini-Hochberg false discovery rate (FDR)[47]. 95% confidence intervals for A^*, acrophase*, and β_0^* were estimated by population-mean cosinor methods[48] deriving from the multivariate F-test.

Variance explained. A proportion of variance explained was calculated as R^2_{UN}=1-SSR/TSS where the G-cosinor model was used to obtain:

$$SSR = (y - \hat{y})^2$$

$$TSS = (y - \beta_0^\star)^2$$

R^2_{DM} was calculated identically to R^2_{UN} except y was first mean subtracted within each individual's data, effectively setting each subject's β_0 to zero and controlling for interindividual variation in β_0. Therefore β_0^* of the G-cosinor models was also set to zero and we proceeded to calculate R^2_{DM}. One oscillating ROI in the GM-MD combined analysis had a low magnitude negative R^2_{UN} estimate which was set to zero for clarity.

Differential acrophase. When BPD and control groups each had significant G-cosinor oscillations, a difference in their acrophases was tested with permutation testing. Acrophase* was obtained for both BPD (acrophase$^*_{BPD}$) and control (acrophase$^*_{CONTROL}$) groups. The minimum difference between them (minimum circular arc length) was then calculated. A permuted null distribution was generated by obtaining the same acrophase difference 10,000 times after shuffling BPD/control labels among subjects and recalculating group-wise acrophase* estimates. The two-sided permutation p-value was the proportion of instances where an absolute acrophase difference from a permuted trial was larger than the real difference.

Acrophase-agnostic test for asynchronous subject-level diurnal oscillations

We implemented a method to complement the G-cosinor test to better utilize the variance explained by each individual within-subject S-cosinor fit. The S-cosinor F-test provided significance for each subject's fitted cosinor curve. As such, individual tests were not influenced by the amplitude/acrophase of other subjects, and were evaluated only by the degree to which they explained the within-subject data. We considered the global null hypothesis that no subjects showed oscillations. Under this null, p-values should follow a uniform distribution, and Fisher's combined probability test[25] considers a likely distribution of p-values (as they would be if the global null were true) with the statistic:

$$\chi^2_{2k} \sim -2\sum_{i=1}^{k} \log(p_i)$$

Where it follows a χ^2 distribution with 2k (k=number of subjects) degrees of freedom. The test is conditional on the independence of subjects and is unweighted with respect to within-subject sample size.

Acrophase variance

Utilizing standard circular statistics[49], with a list of acrophases (θ in radians), an estimate of their mean and variance was obtained by representing each of them as a point, u(C,S), on the unit circle as:

$$u(C,S) = (\cos(\theta), \sin(\theta))$$

The mean (centroid) of these points was obtained as:

$$\bar{u}(\bar{C},\bar{S}) = (\frac{1}{k}\sum_{i=1}^{k}\cos(\theta_i), \frac{1}{k}\sum_{i=1}^{k}\sin(\theta_i))$$

Then, the length of is a measure of acrophase consistency:

$$\bar{R} = \sqrt{\bar{C}^2 + \bar{S}^2}$$

where 1 indicates all acrophases were identical, and conversely, circular variance is and is bounded from 0-1. The mean acrophase was obtained from the direction of as .

Differential acrophase variance. Acrophase variance for both BPD ($_{BPD}$) and control ($_{CONTROL}$) groups were calculated as above. The difference between them (BPD controls) was calculated. A permuted null distribution was generated by obtaining the same acrophase variance difference 10,000 times after shuffling BPD and control labels among subjects and recalculating group-wise acrophase variance estimates. The one-sided permuted p-value was the proportion of instances where the permuted acrophase variance difference was greater than the real difference.

Plotting conventions

Approximate dark times are shown as midnight to 8:00 for all relevant visualizations.

Code Availability

Statistical analysis was performed in R ver. 4.1.3. The code archive fully implements the statistical methods and will be made publicly available upon publication.

Data Availability

Processed ROI data, and whole brain mean values will be made available upon publication on a suitable platform (e.g. Figshare, Zenodo, Dryad) along with intermediate statistics of individual subject fits and ROI fits. Actigraphy data and weight data will also be made available upon publication.

Acknowledgements

We thank the MRI technologists: Anusha Ravichandran, Hillary Bruce, Garry Detzler, and Valerie MacDonald for data collection; CAMH Epigenetics lab staff: Akhil Nair, Miki Susic, Michael Sherman, Richie Jeremian, Edward Oh, Aiping Zhang, William Che, Sasha Ebrahimi, Jeff Villamil for assistance with various parts of the project; Anthony Randal McIntosh for his comments on the manuscript. This project received funding from European Social Fund (project No 09.3.3-LMT-K-712-17-0008) under grant agreement with the Research Council of Lithuania (LMTLT). The project was also supported by grants from Brain Canada and the CAMH Foundation, Project #554, from the Canadian Institutes of Health Research: TGH-158223 and PJT-148719, and the Krembil Foundation (CAMH Foundation Project #186).

Contributions

A.P. conceived the idea of testing diurnal rhythmicity in the brain. N.J.L., S.C. and A.P. designed the overall study protocol and MRI acquisition details. S.C. calculated the qT1 maps. T.L. was responsible for the image processing. M.C., T.L. and N.J.L. conducted the data analyses. A.M. was responsible for the study logistics and conducted in-depth literature reviews. All authors participated in the writing and editing of the manuscript.

Ethics declarations

Competing interests

The authors declare no competing interests.

References

1. Hastings, M. H., Maywood, E. S. & Brancaccio, M. Generation of circadian rhythms in the suprachiasmatic nucleus. *Nat. Rev. Neurosci.* **19**, 453–469 (2018).
2. Logan, R. W. & McClung, C. A. Rhythms of life: circadian disruption and brain disorders across the lifespan. *Nat. Rev. Neurosci.* **20**, 49–65 (2019).
3. Reppert, S. M. & Weaver, D. R. Coordination of circadian timing in mammals. *Nature* **418**, 935–941 (2002).
4. Mure, L. S. *et al.* Diurnal transcriptome atlas of a primate across major neural and peripheral tissues. *Science* **359**, (2018).
5. Ketchesin, K. D. *et al.* Diurnal rhythms across the human dorsal and ventral striatum. *Proc. Natl. Acad. Sci. U. S. A.* **118**, (2021).
6. DiNuzzo, M. & Nedergaard, M. Brain energetics during the sleep–wake cycle. *Curr. Opin. Neurobiol.* **47**, 65–72 (2017).
7. Plumel, M. *et al.* Circadian Analysis of the Mouse Cerebellum Proteome. *Int. J. Mol. Sci.* **20**, (2019).
8. Hodkinson, D. J. *et al.* Circadian and homeostatic modulation of functional connectivity and regional cerebral blood flow in humans under normal entrained conditions. *J. Cereb. Blood Flow Metab.* **34**, 1493–1499 (2014).
9. Elvsåshagen, T. *et al.* Cerebral blood flow changes after a day of wake, sleep, and sleep deprivation. *Neuroimage* **186**, 497–509 (2019).
10. Nakamura, K. *et al.* Diurnal fluctuations in brain volume: Statistical analyses of MRI from large populations. *Neuroimage* **118**, 126–132 (2015).
11. Trefler, A. *et al.* Impact of time-of-day on brain morphometric measures derived from T1-weighted magnetic resonance imaging. *Neuroimage* **133**, 41–52 (2016).
12. Jiang, C. *et al.* Diurnal microstructural variations in healthy adult brain revealed by diffusion tensor imaging. *PLoS One* **9**, e84822 (2014).
13. Elvsåshagen, T. *et al.* Widespread changes in white matter microstructure after a day of waking and sleep deprivation. *PLoS One* **10**, e0127351 (2015).
14. Elvsåshagen, T. *et al.* Evidence for cortical structural plasticity in humans after a day of waking and sleep deprivation. *Neuroimage* **156**, 214–223 (2017).
15. Voldsbekk, I. *et al.* Evidence for wakefulness-related changes to extracellular space in human brain white matter from diffusion-weighted MRI. *Neuroimage* **212**, 116682 (2020).
16. Kaufmann, T. *et al.* The brain functional connectome is robustly altered by lack of sleep. *Neuroimage* **127**, 324–332 (2016).
17. Thomas, C. *et al.* Impact of time-of-day on diffusivity measures of brain tissue derived from diffusion tensor imaging. *Neuroimage* **173**, 25–34 (2018).
18. Muto, V. *et al.* Local modulation of human brain responses by circadian rhythmicity and sleep debt. *Science* **353**, 687–690 (2016).
19. Oh, E. S. & Petronis, A. Origins of human disease: the chrono-epigenetic perspective. *Nat. Rev. Genet.* **22**, 533–546 (2021).
20. Oh, G. *et al.* Circadian oscillations of cytosine modification in humans contribute to epigenetic variability, aging, and complex disease. *Genome Biol.* **20**, 2 (2019).
21. McClung, C. A. How might circadian rhythms control mood? Let me count the ways. *Biol. Psychiatry* **74**, 242–249 (2013).
22. Cornelissen, G. Cosinor-based rhythmometry. *Theor. Biol. Med. Model.* **11**, 16 (2014).
23. Young, R. C., Biggs, J. T., Ziegler, V. E. & Meyer, D. A. A rating scale for mania: reliability, validity and sensitivity. *Br. J. Psychiatry* **133**, 429–435 (1978).
24. Buysse, D. J., Reynolds, C. F., 3rd, Monk, T. H., Berman, S. R. & Kupfer, D. J. The Pittsburgh Sleep Quality Index: a new instrument for psychiatric practice and research. *Psychiatry Res.* **28**, 193–213 (1989).
25. Fisher, R. A. Statistical Methods for Research Workers (Oliver and Boyd, Edinburgh, UK). (1925).
26. Cugini, P. *et al.* Circadian rhythm of some parameters of body composition in the elderly investigated by means of bioelectrical impedance analysis. *Eat. Weight Disord.* **7**, 182–189 (2002).
27. Duning, T. *et al.* Dehydration confounds the assessment of brain atrophy. *Neurology* **64**, 548–550 (2005).

28. Nakamura, K., Brown, R. A., Araujo, D., Narayanan, S. & Arnold, D. L. Correlation between brain volume change and T2 relaxation time induced by dehydration and rehydration: implications for monitoring atrophy in clinical studies. *Neuroimage Clin* **6**, 166–170 (2014).
29. Glasser, M. F. *et al.* A multi-modal parcellation of human cerebral cortex. *Nature* **536**, 171–178 (2016).
30. Fischl, B. *et al.* Whole brain segmentation: automated labeling of neuroanatomical structures in the human brain. *Neuron* **33**, 341–355 (2002).
31. Mori, S. *et al.* Stereotaxic white matter atlas based on diffusion tensor imaging in an ICBM template. *Neuroimage* **40**, 570–582 (2008).
32. Pigeon, W. R., Bishop, T. M. & Krueger, K. M. Insomnia as a Precipitating Factor in New Onset Mental Illness: a Systematic Review of Recent Findings. *Curr. Psychiatry Rep.* **19**, 44 (2017).
33. Harvey, A. G., Talbot, L. S. & Gershon, A. Sleep Disturbance in Bipolar Disorder Across the Lifespan. *Clin. Psychol.* **16**, 256–277 (2009).
34. Wolfers, T. *et al.* Mapping the Heterogeneous Phenotype of Schizophrenia and Bipolar Disorder Using Normative Models. *JAMA Psychiatry* **75**, 1146–1155 (2018).
35. Gottlieb, J. F. *et al.* The chronotherapeutic treatment of bipolar disorders: A systematic review and practice recommendations from the ISBD task force on chronotherapy and chronobiology. *Bipolar Disord.* **21**, 741–773 (2019).
36. Sheehan, D. V. *et al.* The Mini-International Neuropsychiatric Interview (M.I.N.I.): the development and validation of a structured diagnostic psychiatric interview for DSM-IV and ICD-10. *J. Clin. Psychiatry* **59 Suppl 20**, 22–33;quiz 34–57 (1998).
37. Chavez, S. Calibrating variable flip angle (VFA)-based T1 maps: When and why a simple scaling factor is justified. *Proceedings of the International Society of Magnetic Resonance in Medicine (ISMRM), Paris, France* 16–21 (2018).
38. Tustison, N. J. *et al.* N4ITK: improved N3 bias correction. *IEEE Trans. Med. Imaging* **29**, 1310–1320 (2010).
39. Reuter, M., Schmansky, N. J., Rosas, H. D. & Fischl, B. Within-subject template estimation for unbiased longitudinal image analysis. *Neuroimage* **61**, 1402–1418 (2012).
40. Tustison, N. J. *et al.* Large-scale evaluation of ANTs and FreeSurfer cortical thickness measurements. *Neuroimage* **99**, 166–179 (2014).
41. Klein, A. & Tourville, J. 101 labeled brain images and a consistent human cortical labeling protocol. *Front. Neurosci.* **6**, 171 (2012).
42. Andersson, J. L. R. & Sotiropoulos, S. N. An integrated approach to correction for off-resonance effects and subject movement in diffusion MR imaging. *Neuroimage* **125**, 1063–1078 (2016).
43. Smith, S. M. *et al.* Tract-based spatial statistics: voxelwise analysis of multi-subject diffusion data. *Neuroimage* **31**, 1487–1505 (2006).
44. Chavez, S. & Stanisz, G. J. A novel method for simultaneous 3D B(1) and T(1) mapping: the method of slopes (MoS). *NMR Biomed.* **25**, 1043–1055 (2012).
45. Desikan, R. S. *et al.* An automated labeling system for subdividing the human cerebral cortex on MRI scans into gyral based regions of interest. *Neuroimage* **31**, 968–980 (2006).
46. Hua, K. *et al.* Tract probability maps in stereotaxic spaces: analyses of white matter anatomy and tract-specific quantification. *Neuroimage* **39**, 336–347 (2008).
47. Benjamini, Y. & Hochberg, Y. Controlling the False Discovery Rate: A Practical and Powerful Approach to Multiple Testing. *J. R. Stat. Soc. Series B Stat. Methodol.* **57**, 289–300 (1995).
48. Bingham, C., Arbogast, B., Guillaume, G. C., Lee, J. K. & Halberg, F. Inferential statistical methods for estimating and comparing cosinor parameters. *Chronobiologia* **9**, 397–439 (1982).
49. Rao Jammalamadaka, S. & Sengupta, A. *Topics in Circular Statistics*. (World Scientific, 2001).

Characteristic	Controls	BPD	*t*	*p*
Age	35 (9.4)	35 (4.7)	0.056	0.96
Weight [kg]	85 (13)	86 (9.8)	0.25	0.80
Height [cm]	180 (5.5)	170 (4.7)	-3.2	0.0053
BMI	26 (3.6)	30 (3.3) 1	2.3	0.044
Consumed caffeine	12/16	8/8	—	0.26
Is smoker	1/16	4/8	—	0.028
Actigraphy acrophase [hr]	16 (1.5)	16 (2.3)	0.056	0.96
Actigraphy amplitude	1.2 (0.35)	1.1 (0.45)	-0.86	0.41
Actigraphy MESOR	2.6 (0.25)	2.5 (0.24)	-0.79	0.45
Actigraphy time-in-bed [hr]	8.0 (1.7)	7.3 (1.5)	-0.85	0.41
Sleep duration [hr/day]	7.1 (0.67) 4	7.2 (1.1)	0.38	0.71
Sleep quality [PSQI]	5.1 (2.6)	6.5 (3.4)	1.0	0.33
Exercise [hr/week]	5.7 (4.9) 4	6.4 (9.8)	0.20	0.85
Body weight acrophase [hr]	24 (2.5)	25 (2.0)	1.0	0.32
Body weight diurnal amplitude [kg]	0.65 (0.29)	0.65 (0.48)	0.029	0.98
Body weight MESOR [kg]	86 (13)	88 (13)	0.41	0.69
Young Mania Rating Scale	—	1.0 (1.5)	—	—

Table 1 | Participant characteristics.
Continuous data are summarized as "mean (SD) #missing" and were tested for group-wise differences with a two-sided Welch's two sample t-test, while binary outcomes were tested with a two-sided Fisher's exact test. "Consumed caffeine" - the participant consumed some caffeine (coffee, tea, soda) at various times and amounts during the on-site portion of the study. "Is smoker" - participant was a smoker/vaper; none consumed nicotine during the scanning session. Exercise and sleep duration were self-reported. Weight diurnal oscillation parameters were estimated for each subject with a S-cosinor model (Methods). Actigraphy-based subject-specific diurnal parameters were estimated from log transformed actigraphy step data and average recorded total daily time-in-bed was obtained directly (Supplementary Fig. 4; Methods).

Whole brain		*Oscillation parameters*			*G-cosinor zero amplitude*	*Effect size*		
	Metric	MESOR [CI]	Amplitude [CI]	Acrophase [CI]	*p*	R^2_{UN}	R^2_{DM}	Units
Controls (n=16)	CBF	63 [51,76]	4.5 [2.0,7.0]	21 [20,23]	0.0088	0.020	0.15	ml/g/min
	GM-MD	0.089 [0.087,0.091]	4.4e-04 [2.3e-04,6.5e-04]	16 [14,18]	0.0025	0.0055	0.20	0.1 mm^2/s
	WM-FA	0.45 [0.44,0.45]	9.9e-04 [3.8e-04,0.0016]	18 [16,21]	0.0034	0.0034	0.084	—
	WM-MD	0.075 [0.074,0.076]	2.4e-04 [1.3e-04,3.5e-04]	13 [11,15]	0.0017	0.0098	0.19	0.1 mm^2/s
	Weight	86 [79,93]	0.55 [0.38,0.72]	24 [23,1]	5.7e-06	4.1e-04	0.38	kg
BPD (n=8)	GM-MD	0.092 [0.089,0.094]	4.8e-04 [2e-04,7.6e-04]	15 [12,19]	0.027	0.0094	0.15	0.1 mm^2/s
	WM-FA	0.45 [0.44,0.45]	0.0019 [0.0012,0.0025]	17 [15,19]	0.0019	0.015	0.23	—
	SA	185 [171,198]	0.52 [0.20,0.84]	3 [1,7]	0.030	8.1e-04	0.14	10^3 mm^2
	Weight	88 [77,99]	0.61 [0.21,1.0]	24 [23,2]	0.034	0.0046	0.37	kg
Combined (n=24)	CBF	59 [50,67]	3.2 [1.3,5.2]	21 [20,23]	0.0090	0.013	0.10	ml/g/min
	GM-MD	0.090 [0.088,0.091]	4.5e-04 [3e-04,6.1e-04]	16 [14,17]	2.9e-05	0.0049	0.18	0.1 mm^2/s
	WM-FA	0.45 [0.44,0.45]	0.0013 [8e-04,0.0018]	17 [16,19]	1.5e-05	0.0059	0.13	—
	WM-MD	0.075 [0.075,0.076]	2.1e-04 [1.3e-04,2.9e-04]	13 [12,15]	0.00012	0.0084	0.18	0.1 mm^2/s
	SA	188 [182,194]	0.31 [0.13,0.49]	4 [1,7]	0.0053	1.7e-04	0.043	10^3 mm^2
	GMV	519 [500,537]	1.3 [0.34,2.3]	6 [3,9]	0.038	5.4e-04	0.048	10^3 mm^3
	Weight	86 [81,92]	0.57 [0.42,0.72]	24 [23,1]	6.1e-07	0.0018	0.38	kg

Regional ranges for FDR q<0.05 ROIs

	Metric	MESOR	Amplitude	Acrophase	% p<0.05 (#/total; # q<0.05)	R^2_{UN}	R^2_{DM}	Units
Controls	CBF	46-82	1.8-9.2	18-23	85.8% (319/372; 289)	0.0062-0.047	0.033-0.21	ml/g/min
	GM-MD	0.073-0.10	4.5e-04-0.0013	14-20	37.9% (141/372; 53)	5.95e-04-0.03	0.052-0.21	0.1 mm^2/s
	WM-MD	0.071-0.085	2.1e-04-0.0013	8-18	26.1% (12/46; 3)	0.0042-0.028	0.096-0.13	0.1 mm^2/s
BPD	WM-FA	0.51-0.67	0.0028-0.0046	15-20	21.7% (10/46; 5)	0.006-0.035	0.084-0.25	—
	CT	2.5	0.062	4	3.6% (13/358; 1)	0.096	0.19	mm
Combined	CBF	42-72	1.7-6.1	18-24	83.3% (310/372; 265)	0.0045-0.034	0.028-0.18	ml/g/min
	GM-MD	0.072-0.11	2.7e-04-0.0015	8-19	55.4% (206/372; 168)	0-0.024	0.024-0.18	0.1 mm^2/s
	WM-FA	0.49-0.66	2.1e-03-0.0029	13-18	34.8% (16/46; 8)	0.0038-0.013	0.046-0.11	—

Table 2 | MRI metrics showing significant G-cosinor results.
G-cosinor parameters and statistics are presented for controls only, BPD patients only, and the combined group. Supplementary Table 2 and Supplementary Table 4 provide statistics and summaries for all metrics.

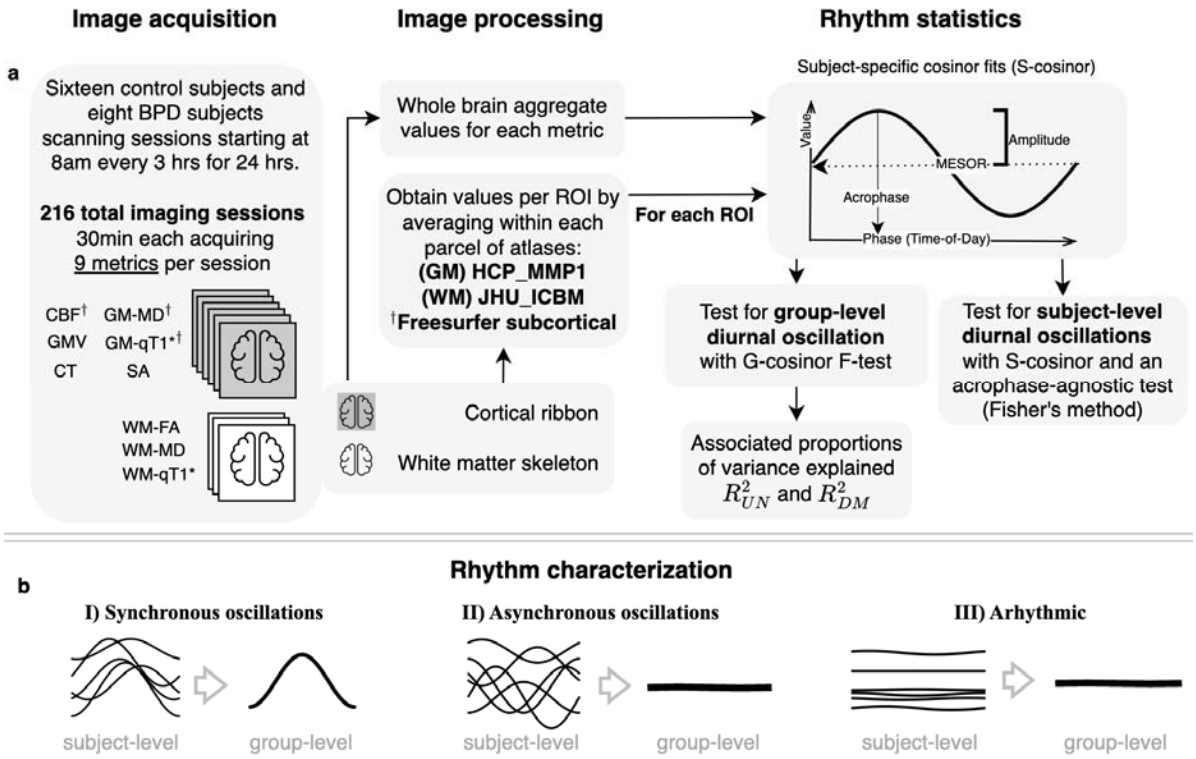

Figure 1 | Pipeline for estimating diurnal oscillations in MRI metrics.
a) Image acquisition (left): Scanning schedule and metrics derived from imaging protocols. Grey brains: grey matter metrics (cortical ribbon, subcortical structures); white brains: metrics from white matter skeleton. **Image processing** (centre): Following registration to template, whole-brain aggregate values were obtained for the whole cortical ribbon and white matter skeleton (Supplementary Fig. 6) as well as parcels based on grey and white matter brain atlases. **Rhythm statistics** (right): Top: for each individual and metric, cosinor modeling produced estimates of the acrophase, amplitude, and MESOR. Bottom: G-cosinor test and an acrophase-agnostic test characterized group-level and subject-level oscillations, respectively and estimated proportion of variance explained by oscillations. **b)** Three rhythmicity scenarios: I) oscillations were present and synchronous across subjects, II) oscillations were present but asynchronous across subjects, and III) oscillations were absent. Asterisk (*): qT1 was acquired for all patients, and 12 of the 16 control subjects. Dagger (†): Additional freesurfer automatic segmentation subcortical ROIs were obtained for these metrics.

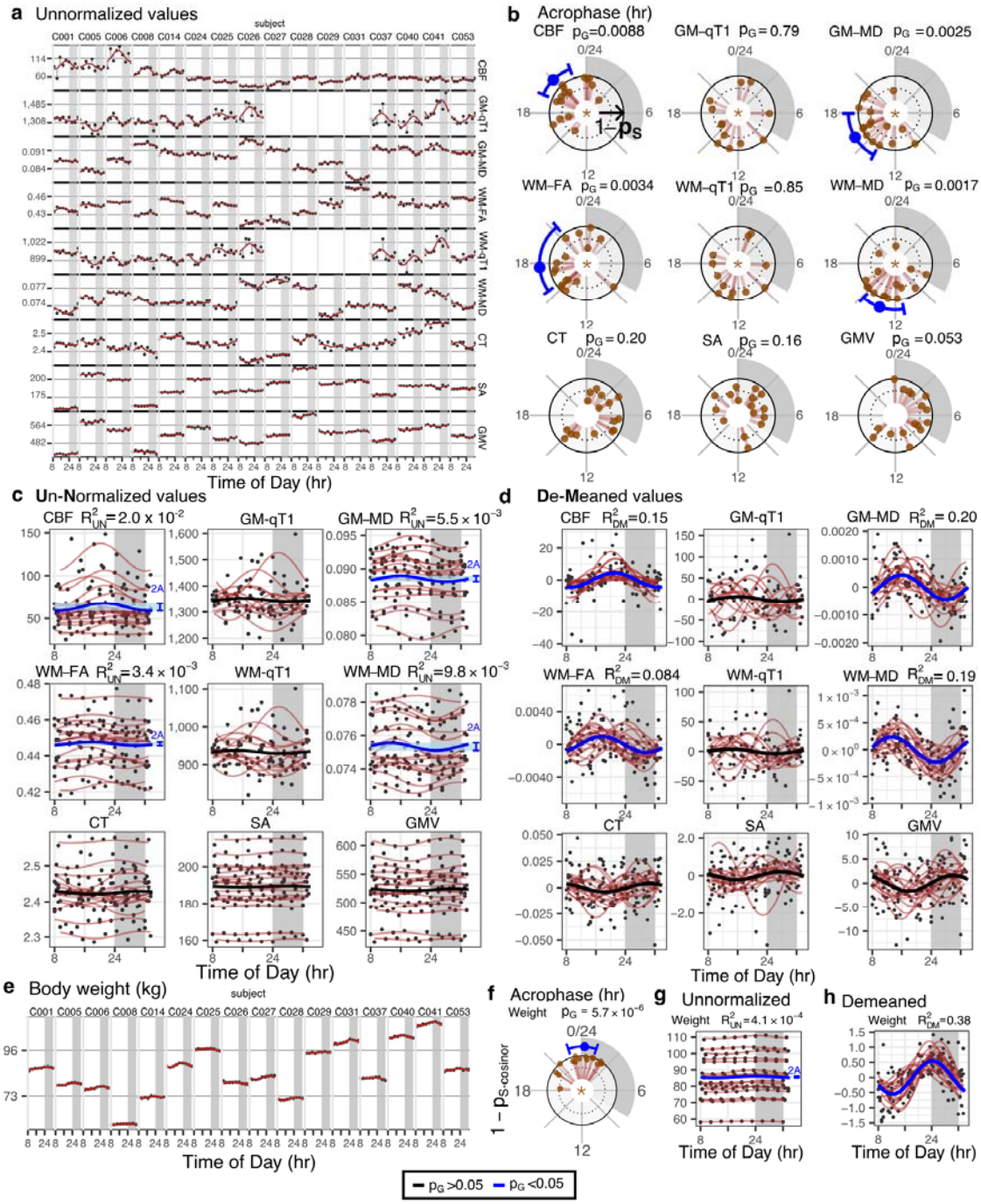

744 **Figure 2 | Diurnal oscillations in the whole brain.**
745 **a)** Metric values (y-axis) over a 24-hr period (x-axis) for each subject (columns) for each of the nine MRI
746 metrics (rows). S-cosinor fit lines are shown with residuals connecting dots to the fit. **b)** Circular plots of
747 S- and G-cosinor acrophases. Rotational axis: time of day (0-24hrs). Brown dots: acrophase for each
748 subject. Radial axis: inverse S-cosinor p-values ($1-p_S$) ranging from zero to one. Blue lines: significant
749 ($p<0.05$) G-cosinor acrophase estimates with corresponding 95% CI. Plot panel titles indicate the G-
750 cosinor p-values (p_G). Panel centres: Star (☆) indicates metrics where the acrophase-agnostic test was
751 significant ($p<0.05$). **c)** Metric values as in (a), grouped by metric, with S-cosinor fit lines in brown, as in
752 (a); G-cosinor curve shown in blue where the blue bracket and shading indicate peak-to-peak amplitude
753 (2*A) of the G-cosinor model. Plot panel titles indicate the proportion of variance explained by the G-

cosinor model in these data (R^2_{UN}). **d)** Within-subject demeaned values (dots) reveal oscillatory effects of the G-cosinor model, represented as thick lines (black, $p>0.05$; blue, $p<0.05$). The S-cosinor fits are shown as brown lines. Plot panel titles indicate the proportion of variance explained by the G-cosinor model on the demeaned data (R^2_{DM}). **a-d)** qT1 was not acquired for four subjects. **e-h)** Identical methods as in (a-d) applied to body weight data.

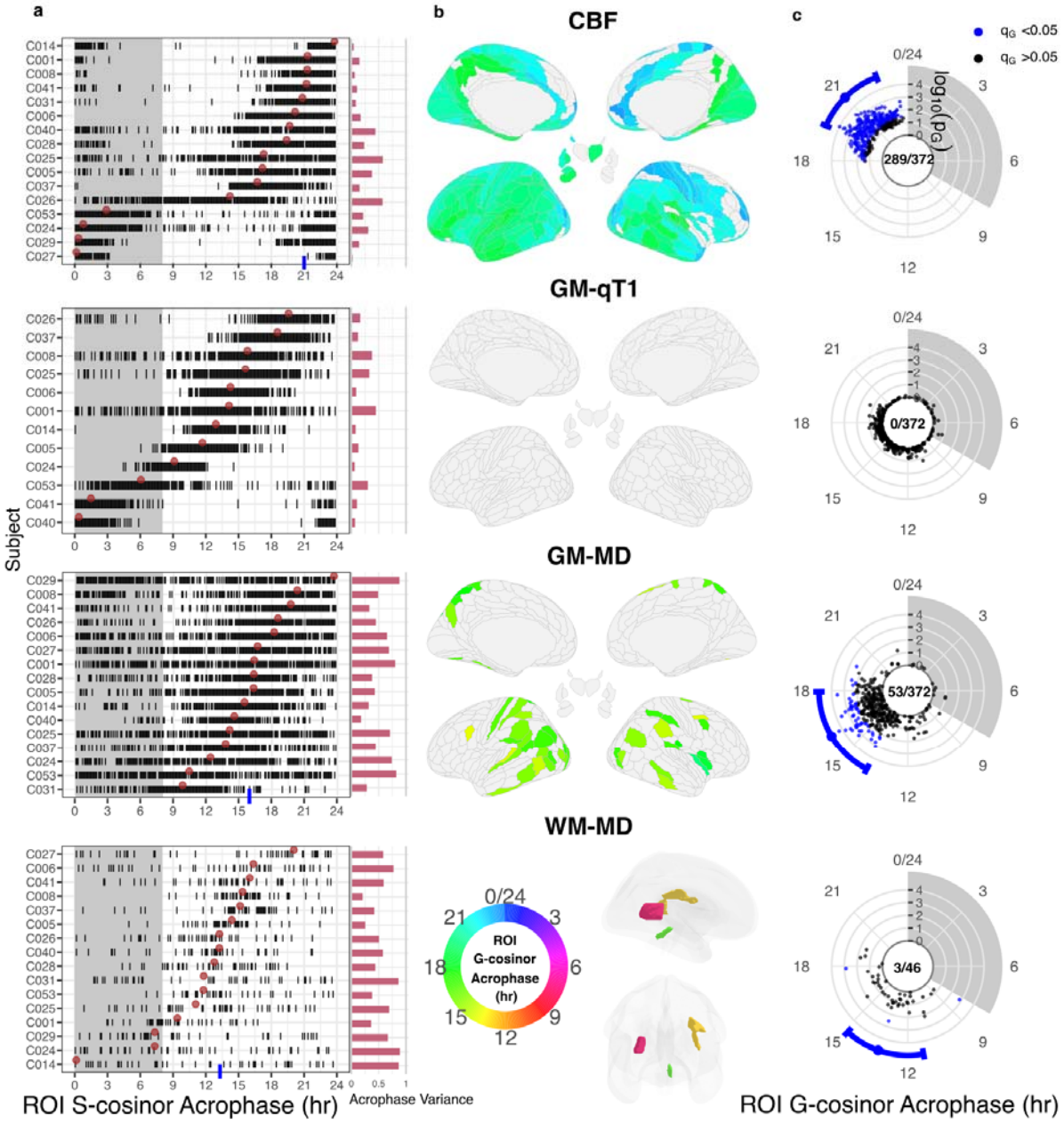

Figure 3 | Regional cosinor statistics for control subjects.
ROI-wise results for CBF, GM-MD, and WM-MD to illustrate significant group-level oscillations, and lack of such in GM-qT1. Each metric is shown in one row as indicated by centre titles. **a)** Left: Subject-level (S-cosinor) acrophase estimates are plotted as vertical ticks for each ROI (x-axis), individually for each subject (y-axis). For each metric, subjects are sorted according to their whole brain subject-level acrophase (brown dots). Blue tick: significant whole-brain G-cosinor acrophase estimate. Right: Red bars indicate each subject's acrophase variance across all ROIs (Methods). **b)** Colour-coded G-cosinor acrophase times for significant ROIs (FDR q<0.05) displayed on brain surfaces. Grey regions were not significant. **c)** Blue dots: estimates of the G-cosinor acrophase for each ROI shown on the rotational axis in polar coordinates where the radial axis is the negative logarithm of the G-cosinor p-value. Blue intervals: significant whole brain acrophases and 95% CI. Panel centres: the number of significant ROIs to total ROIs. All 9 MRI metrics are presented in Supplementary Fig. 2.

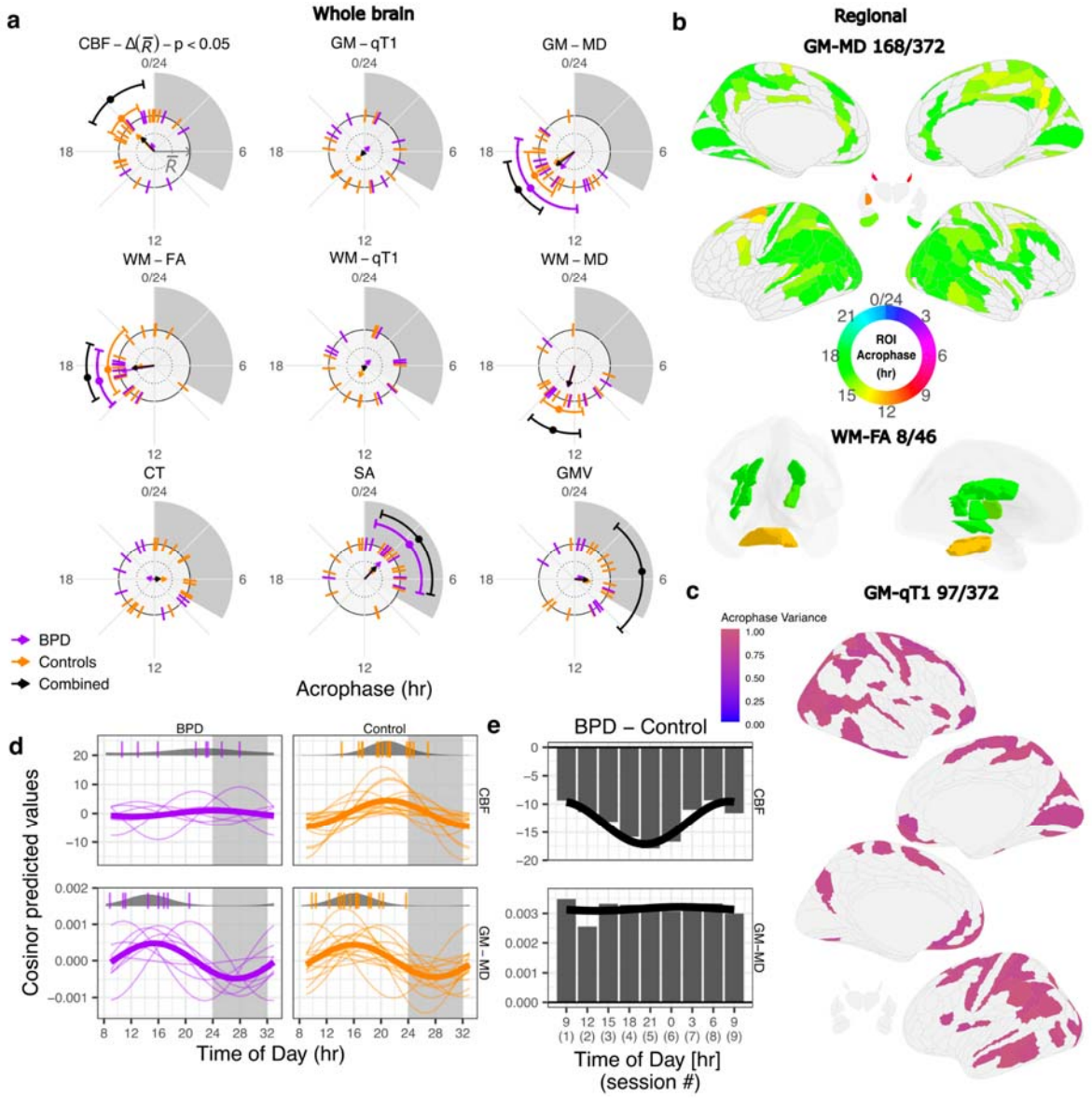

Figure 4 | Diurnal oscillations in BPD, control, and the combined group.
a) Acrophases of whole-brain oscillations (G-cosinor p<0.05) and confidence intervals shown on outer orbit. S-cosinor acrophases for each subject are shown as ticks. Each arrow points in the direction of the mean acrophase across control subjects (orange arrow), BPD patients (purple), or both (black) and its length represents a measure of acrophase consistency across subjects (1 − acrophase variance). The significant difference in acrophase consistency between patients and controls for CBF is indicated in the panel title. **b)** Acrophases of regional oscillations (G-cosinor FDR q<0.05) for GM-MD and WM-FA in the combined group (as in Figure 3b) illustrating the increased number of oscillating ROIs relative to controls-only. **c)** Significant ROIs for GM-qT1 in the combined group (acrophase-agnostic test FDR q<0.05) coloured according to their log transformed p value. **d)** S-cosinor models (thin lines) on the demeaned data in CBF and GM-MD with G-cosinor model (thick line). Top of each panel: S-cosinor acrophases shown as ticks overlaid on probability density plots (circular normal) estimated for each group. **e)** Between-group differences in CBF and GM-MD at each of the nine scanning sessions, highlighting the impact of the oscillation differences between BPD patients and controls (x-axis: average session time). A cosinor fit to the differences is shown as a black line.

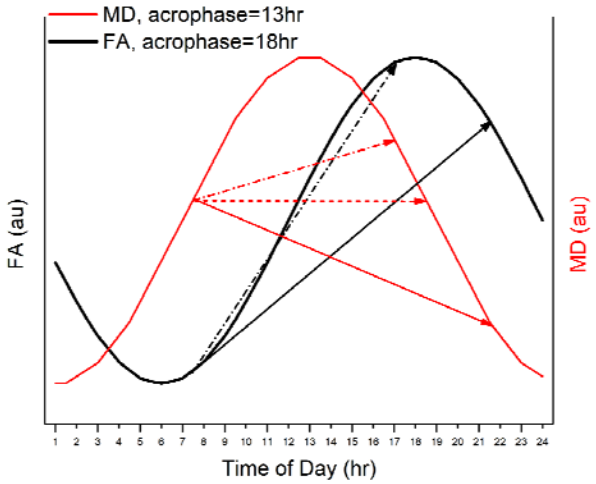

Figure 5 | Group-level cosinor models for FA and MD in the white matter skeleton (controls only). For WM-MD (red), acrophase was at mid-day (13hrs). For WM-FA (black), acrophase was in late afternoon (18hrs). Arrows indicate possible time-of-day effects. Solid arrows: Scans at 7:30 and 21:30; Dash-dotted arrows: Scans at 7:30 and 17:00; Dotted arrow (MD only): Scans at 7:30 and 18:30. Acrophases from Table 2.